Cooperation and Coordination Transportation for Nonholonomic Mobile Manipulators: A Distributed Model Predictive Control Approach

Dongdong Qin, Jinhui Wu, Andong Liu, Wen-An Zhang, *Member, IEEE*, and Li Yu, *Member, IEEE*

***Abstract*—This article addresses the problem of cooperation and coordination transportation for decoupling nonholonomic mobile manipulators (NMMs) in a workspace with obstacles. We propose a distributed model predictive control (MPC) approach for a team of NMMs to transport a target object while satisfying significant constraints and limitations, such as the feasible state and control input constraints, parameter synchronization constraints, and obstacles within the workspace. First, under the framework of the decoupling dynamics, an auxiliary dynamics model for task-space end-effectors and null-space mobile bases is obtained by the nonlinear feedback technique based on the Euler–Lagrange description of the NMMs. Using the modified virtual structure method, the cooperation and coordination transportation problem for NMMs is simplified as two independent synchronization tracking control problems for task-space end-effectors and null-space mobile bases. A distributed constrained optimization problem is established by taking the parameter synchronization and system constraints into the cost function. A general projection neural network (GPNN) approach is employed to solve the optimization problem and obtain the optimal control input. Moreover, a sufficient condition that guarantees the stability of the closed-loop system is further developed. Simulation results show that the proposed cooperation and coordination transportation strategy is feasible and effective.**

***Index Terms*—Cooperation and coordination transportation, distributed model predictive control (MPC), general projection neural network (GPNN), modified virtual structure, nonholonomic mobile manipulators (NMMs).**

I. Introduction

In RECENT years, multirobot cooperative manipulation has become an important research topic for increasing efficiency, robustness, and flexibility in industrial assembly, warehousing logistics, and environmental exploration [1]–[5]. Compared with a mobile robot or manipulator, mobile manipulator merges the manipulator's dexterity with the mobile platform's increased workspace capabilities and has become a popular tool in cooperative manipulation [6]–[8]. As one of the prototypical problems of multirobot cooperative manipulation, cooperative transportation refers to a team of physically nonholonomic mobile manipulators (NMMs) collaboratively transporting an object from an initial position to the desired position with interaction, which has attracted considerable attention [9]–[12].

Since the mobile manipulator is a nonlinear and strongly coupled mechanical system, designing an efficient and feasible cooperation control strategy for NMMs has been challenging [13], [14]. In [15], a hybrid control strategy is developed for the motion/force control for the coordinated multiple mobile manipulators system, considering the actuator dynamics. In [16], by using an adaptation-based estimation law to estimate the desired local trajectory, a fully distributed adaptive control strategy is proposed to achieve motion synchronization of the networked mobile manipulators regardless of the kinematic and dynamic uncertainties in both the mobile manipulators and the tightly grasped object. In [17], a novel cooperative control method for mobile manipulators in the context of the distributed formation control integrated with constrained optimization is developed, where the cost function and safety constraints are designed to quantify the mobility and manipulability of the mobile manipulators. Cooperative transportation by the networked mobile manipulators in unknown environments is addressed in [18]. Further research has investigated the cooperative transportation control for mobile manipulators in [19] by the distributed optimization approach. Although the stability and tracking performance can be guaranteed, the works mentioned above only consider the cooperation between the robots. To improve the flexibility of cooperation transportation for the networked mobile manipulators, the coordination between end-effector and mobile bases of NMM is considered in [20], and decoupling dynamics are utilized to enable the task (end-effector) and null space (mobile base) of the mobile manipulators to complete the different tasks, respectively. However, most of the works mentioned above are based on nonoptimal control methods. They cannot achieve synchronization of the position and velocity of the networked mobile manipulators. In addition, the feasible state and control input constraints of the NMMs are not considered.

Distributed model predictive control (MPC) is an appropriate and effective optimal control method for constrained large-scale robot systems. It has obtained considerable attention

Manuscript received 29 November 2021; revised 29 May 2022; accepted 1 July 2022. Date of publication 20 July 2022; date of current version 16 January 2023. This work was supported in part by the National Natural Science Foundation of China under Grant 61973275; in part by the Zhejiang Provincial Natural Science Foundation of China under Grant LD21F030002; and in part by the Fundamental Research Funds for the Provincial Universities of Zhejiang under Grant RF-A2020004. This article was recommended by Associate Editor G. Wen. *(Corresponding author: Andong Liu.)*

The authors are with the College of Information Engineering, Zhejiang Provincial United Key Laboratory of Embedded Systems, Zhejiang University of Technology, Hangzhou 310023, China (e-mail: lad@zjut.edu.cn).

Color versions of one or more figures in this article are available at https://doi.org/10.1109/TSMC.2022.3189007.

Digital Object Identifier 10.1109/TSMC.2022.3189007

2168-2216 © 2022 IEEE. Personal use is permitted, but republication/redistribution requires IEEE permission.
See https://www.ieee.org/publications/rights/index.html for more information.

Authorized licensed use limited to: b-on: Universidade de Lisboa Reitoria. Downloaded on October 20,2024 at 11:23:04 UTC from IEEE Xplore. Restrictions apply.

for its tractable computation and flexible system structure [21]–[23]. A distributed MPC strategy is presented in [24] for linear systems with additive uncertainty and coupled probabilistic constraints, where coupled probabilistic constraints are solved nonconservatively in a distributed way. In [25], a nonlinear MPC strategy that guarantees the navigation of the object to the desired pose in a bounded workspace with obstacles is proposed to address the cooperative transportation of robotic agents with certain input saturations. Moreover, a distributed MPC approach is proposed in [26] to solve the problem of cooperative object transportation for multiple underwater vehicle manipulator systems in a constrained workspace involving static obstacles while avoiding significant constraints and limitations, such as kinematic and representation singularities, obstacles within the workspace, joint limits, and control input saturation. One of the main focuses of implementing the distributed MPC is computational efficiency. It will be degraded by the computational loads generated by the expansion of the system's state and the increase in prediction horizon, especially in a large-scale distributed cooperative system. Several neurodynamic optimization methods have been used to solve the distributed convex and pseudoconvex optimization problem for their apparent advantages, such as parallel computed nature, global robustness convergence, and convenience of hardware implementation. In [27], a primal–dual neural network (PDNN) is applied to solve the quadratic programming (QP) problem resulting from the discussed MPC optimization problem, and its realization by MATLAB Simulink is investigated in [28]. A general projection neural network (GPNN) is investigated in [29] and [30], and it is used to solve the distributed constrained QP problem in [31], and other related works of projection and duality neural network can also be found in [32]. In this article, to improve the online computational efficiency of the distributed MPC algorithm, the GPNN is implemented to solve the constrained QP problem to obtain the optimal control input.

Inspired by the above discussion, a cooperation and coordination transportation problem for the decoupling NMMs with the feasible state and input constraints is investigated by using the distributed MPC approach and the modified virtual structure method. The main contributions of this article are formulated as follows.

1) For cooperation and coordination transportation of the networked NMMs, a decoupling NMMs' model is established where the task-space end effector is used to cooperatively transport the target object from the initial position to the desired position, and the null-space mobile base is used to perform obstacle avoidance task while transporting the target object along the reference path. Compared with cooperation transportation in [16] and [17], the coordination between the end-effector and mobile bases is considered to enhance the flexibility of cooperation transportation.
2) For motion coordination, a novel updating law of the path parameter for the modified virtual structure is designed using the error of the position and velocity of the NMM. Different from the updating law in [23] and [27], our proposed updating law is more suitable for practical situations with less conservative. By introducing the path parameter synchronization constraint into the cost function, the synchronization of the position and velocity of the networked mobile manipulators can be achieved.
3) A GPNN-based distributed MPC strategy is proposed for the cooperation and coordination transportation of the decoupling NMMs with the feasible state and input constraints, and a sufficient condition guaranteeing the closed-loop system's stability is given. Compared with [16], [18], and [20], an optimal synchronization tracking controller is obtained to drive the decoupling NMMs to achieve the transportation task.

II. Problem Description

In this section, a decoupled modeling process is formulated for NMM subjected to the external force disturbance. Moreover, a closed-chain model-based contribution principle is proposed to estimate this force disturbance exerted by the target object.

A. NWW Modeling

Based on the Euler–Lagrange equations, the dynamics of NMM i can be described as follows [33]:

$$M_{q_i}(q_i)\ddot{q}_i + \Theta_{q_i}(q_i, \dot{q}_i) = B_{q_i}(q_i)\tau_i + f_i(q_i) \tag{1}$$

$$f_i(q_i) = A_i^T(q_i)\lambda_i \tag{2}$$

where M_{q_i} is the positive-definite inertia matrix, $\Theta_{q_i}(q_i, \dot{q}_i)$ is a blend term that includes the Coriolis or Centrifugal forces, and the gravitational forces. q_i, $\dot{q}_i$, and $\ddot{q}_i$ are the generalized position, velocity, and acceleration vectors, respectively. $B_{q_i}(q_i)$ is a known constant matrix related to the system's geometry structure, and τ_i is the input torque vector. (2) describes the generalized constraint forces resulting from the nonholonomic constraints.

To eliminate the influence of the nonholonomic constraints forces, $\dot{q}_i = S(q_i)\dot{\theta}_i$ and its derivative are substituted into (1), and the dynamics of NMM with external force disturbance can be rewritten as

$$M_{\theta_i}(q_i)\ddot{\theta}_i + C_{\theta_i}(q_i, \dot{q}_i)\dot{\theta}_i + G_{\theta_i}(q_i) = \tau_{\theta_i} + \tau_{e_i} \tag{3}$$

where $\dot{\theta}_i = [\dot{\theta}_R, \dot{\theta}_L, \dot{\theta}_1, \ldots, \dot{\theta}_n]^T$ is the generalized joint velocity vector, $\dot{\theta}_R$ and $\dot{\theta}_L$ represent the right and left wheel's angular velocities, respectively, and $\dot{\theta}_k$, $k = 1, \ldots, n$ is the angular velocity of the kth joint of manipulator. $M_{\theta_i} = S_i^T M_{q_i} S_i$, $C_{\theta_i} = S_i^T M_{q_i} \dot{S}_i$, $G_{\theta_i} = S_i^T \Theta_{q_i}$. $\tau_{\theta_i} = S_i^T B_{q_i} \tau_i$ is the generalized joint input torque vector. τ_{e_i} is the external force disturbance exerted on the end effector by the target object.

B. Task-Space and Null-Space Decoupling

The kinematic relation between the task-space velocities and the joint-space velocities of the NMM i is given as

$$\dot{X}_{m_i} = J_{m_i}\dot{\theta}_i \tag{4}$$

where $X_{m_i} = [x_{m_i}, y_{m_i}]^T$ is the Cartesian coordinates of the end effector in $x - y$ position, and J_{m_i} is the Jacobian matrix

Authorized licensed use limited to: b-on: Universidade de Lisboa Reitoria. Downloaded on October 20,2024 at 11:23:04 UTC from IEEE Xplore. Restrictions apply.

from the joint velocities to the end-effector velocities. As the mapping of the end-effector velocities to the joint velocities is not unique, the general solution of $\dot{\theta}_i$ is define as [24]

$$\dot{\theta}_i = J_{m_i}^{+}\dot{X}_{m_i} + N_i\dot{\theta}_i \tag{5}$$

where $J_{m_i}^{+}$ is the generalized inverse of the Jacobian matrix J_{m_i}, and N_i is its null space. By taking the derivative of (5), we can obtain

$$\ddot{\theta}_i = J_{m_i}^{+}\ddot{X}_{m_i} + \dot{J}_{m_i}^{+}\dot{X}_{m_i} + N_i\ddot{\theta}_i + \dot{N}_i\dot{\theta}_i \tag{6}$$

where the first two terms on the right of (6) represent the joint acceleration, and the other two terms describe the mobile accelerations. Similarly, the relationship between the generalized joint input torque τ_{θ_i} and the task-space force F_i is given as follows:

$$\tau_{\theta_i} = J_{m_i}^{T}F_i + N_i^{T}\tau_{n_i} \tag{7}$$

where τ_{n_i} is an arbitrary joint torque vector. By substituting (5), (6), and (7) into (3), and simplifying the obtained equation with $N_i = I - J_{m_i}^{+}J_{m_i}$, we have

$$J_{m_i}^{T}F_i + N_i^{T}\tau_{n_i} = \Theta_1 + \Theta_2 + \Theta_3 \tag{8}$$

where $\Theta_1 = N_i^{T}(M_{\theta_i}N_i\ddot{\theta}_i + C_{\theta_i}\dot{\theta}_i + G_{\theta_i} - \tau_{e_i})$ represents the input torques acting on the null space, $\Theta_2 = J_{m_i}^{T}J_{m_i}^{+T}(M_{\theta_i}J_{m_i}^{+}(\ddot{X}_{m_i} - \dot{J}_{m_i}\dot{\theta}_i)) + C_{\theta_i}\dot{\theta}_i + G_{\theta_i} - \tau_{e_i}$ represents the task-space force, and $\Theta_3 = J_{m_i}^{T}J_{m_i}^{+T}M_{\theta_i}N_i\ddot{\theta}_i + N_i^{T}M_{\theta_i}J_{m_i}^{+}(\ddot{X}_{m_i} - \dot{J}_{m_i}\dot{\theta}_i)$ represents the coupling forces and torques. The decomposition between the end-effector motion and the internal motion can be achieved by setting $J_{m_i}^{T}J_{m_i}^{+T}M_{\theta_i} = 0$ and $N_i^{T}M_{\theta_i}J_{m_i}^{+} = 0$, which are supported by the condition that $J_{m_i}^{+} = M_{\theta_i}^{-1}J_{m_i}^{T}(J_{m_i}M_{\theta_i}^{-1}J_{m_i}^{T})^{-1}$. Based on the analysis above, the decoupling dynamics of the NMM i in task space are obtained as

$$\bar{M}_i\ddot{X}_{m_i} + \bar{C}_i\dot{X}_{m_i} + \bar{G}_i = F_i + F_{e_i} \tag{9}$$

where $\bar{M}_i = (J_{m_i}M_{\theta_i}^{T}J_{m_i}^{T})^{-1}$, $\bar{C}_i\dot{X}_{m_i} = J_{m_i}^{+}C_{\theta_i}\dot{\theta}_i - \bar{M}_{m_i}\dot{J}_{m_i}\dot{\theta}_i$, and $\bar{G}_i = J_{m_i}^{+T}G_{\theta_i}$. $F_i = J_{m_i}^{+T}\tau_{\theta_i}$ is the task-space control vector, and $F_{e_i} = J_{m_i}^{+T}\tau_{e_i}$ is the external force disturbance estimated in the following section.

Define u_{mi} and u_{ni} as the new task-space controller and the null-space controller, respectively, the control input τ_{θ_i} can be decoupled as follows:

$$\begin{aligned}\tau_{\theta_i} = {} & J_{m_i}^{T}\bar{M}_i\left(u_{m_i} - \dot{J}_{m_i}\dot{\theta}_i\right) + N_i^{T}M_{\theta_i}\left(u_{n_i} + \dot{J}_{m_i}^{+}\dot{X}_{m_i}\right) \\ & + C_{\theta_i}\dot{\theta}_i + G_{\theta_i} + J_{m_i}^{T}F_{e_i}.\end{aligned} \tag{10}$$

It can be observed from (10) that the variables representing the position and velocity of NMM are the current states, and both are uncontrollable. Thus, we consider the accelerations $\ddot{X}_{m_i}$ in task space and $\ddot{\theta}_{b_i}$ in null space as the controlled states.

By substituting (10) into (8), the decoupled task-space closed-loop dynamics can be expressed as

$$\ddot{X}_{m_i} = u_{m_i}. \tag{11}$$

Meanwhile, the null-space closed-loop dynamics is obtained as

$$\ddot{\theta}_i = u_{n_i} + \dot{J}_{m_i}^{+}\dot{X}_{m_i} \tag{12}$$

where $u_{n_i} = [\tau_{n_{b_i}}, \tau_{n_{m_i}}]^{T}$. $\tau_{n_{b_i}}$ is the null-space control vector, and $\tau_{n_{m_i}}$ is the task-space control vector. Since $\tau_{n_{m_i}}$ has been considered in task space, for convenience, we set $\tau_{n_{m_i}} = 0$.

Under the frame of the decoupling dynamics, the simplified dynamic model satisfying the nonholonomic constraints for the mobile base of the NMM i can be expressed as follows [33]:

$$M_{\theta_{b_i}}\ddot{\theta}_{b_i} + C_{\theta_{b_i}}\dot{\theta}_{b_i} = B_{\theta_{b_i}}\tau_{n_{b_i}} \tag{13}$$

where $M_{\theta_{b_i}}$, $C_{\theta_{b_i}}$, and $B_{\theta_{b_i}}$ are the inertial matrix, the Coriolis and Centrifugal force matrix, and the gravitational force matrix, respectively. By substituting the nonlinear feedback input $\tau_{n_{b_i}} = B_{\theta_{b_i}}^{-1}(M_{\theta_{b_i}}u_{\theta_{b_i}} + C_{\theta_{b_i}}\dot{\theta}_{b_i})$ into (13), we can obtain the relationship between the left- and right-wheels' acceleration and the auxiliary control input, such that

$$\ddot{\theta}_{b_i} = u_{\theta_{b_i}}. \tag{14}$$

According to the velocity relationship $\dot{X}_{b_i} = J_{b_i}\dot{\theta}_i$, (14) can be transformed as the following equation employed to regulate the position of the mobile base in null space, given as:

$$\ddot{X}_{b_i} = u_{n_{b_i}} \tag{15}$$

where $X_{b_i} = [x_{b_i}, y_{b_i}]^{T}$, and $u_{n_{b_i}} = J_{b_i}u_{\theta_{b_i}} + \dot{J}_{b_i}\dot{\theta}_i$.

Based on the above analysis, the motion of NWW is decoupled as a task-space motion for end effector, and a null-space motion for mobile base, the controller u_{m_i} in (11) and u_{n_i} in (15) can be designed to drive end effector and mobile base to implement different tasks.

C. Internal Force Analysis

In cooperation and coordination transportation, the motion of NMMs is coupled in task space by a target object. It leads to an undesired effect on the motion of the NMMs by exerting a force disturbance on the end effectors. Thus, it is necessary to consider the external forces τ_{e_i} in the motion of the NMMs. In this section, a closed-chain model is reported to give a reasonable approximation of the force exerted on the end effector by the target object. To begin with, we consider the following dynamic model of the target object [34]:

$$M_o\ddot{X}_o + C_o\dot{X}_o + G_o = F_o \tag{16}$$

where $\ddot{X}_o$ and X_o are the velocity and position vectors of the target object. M_o, C_o, and G_o are the coefficient matrices, which are assumed to known. F_o is the resultant force acting on the target object by NMMs. For force analysis of objects, we have

$$F_{ce_i} = J_{ce_i}^{T}F_{e_i} = \tau_{\text{int}} + \tau_{o_i} \tag{17}$$

$$F_o = -\sum F_{ce_i} \tag{18}$$

where F_{ce_i} denotes the force exerted on the end effector by the target object, and $J_{ce_i}^{T}$ is jacobian matrix from the target centroid to the end effector of the NMM i. τ_{int} is the internal force acting on the object and $\sum \tau_{\text{int}} = 0$. τ_{o_i} denotes the force acting on the movement of the target. By taking (17) and (18) into (16), one has

$$M_o\ddot{X}_o + C_o\dot{X}_o + G_o = -\sum_{i\in\Omega}\tau_{o_i} \tag{19}$$

Authorized licensed use limited to: b-on: Universidade de Lisboa Reitoria. Downloaded on October 20,2024 at 11:23:04 UTC from IEEE Xplore. Restrictions apply.

where Ω represents the set of NMMs. Suppose that the contribution of the NMM i to the target motion can be described by

$$c_i(t) = \frac{\tau_{o_i}}{\sum_{j\neq i\in\Omega}\tau_{o_j}} \tag{20}$$

where $c_i(t)$ is the contribution ratio of the end effector of the NMM i. Obviously, it is a time-varying parameter complying with the state of the target object. A simple example is considered that the system consisting by the target object and the NMMs is in equilibrium, and c_i is a fixed constant. It means that the force exerted on each end effector by the target object is uniformly. Moreover, substituting (19) into (18), τ_{o_i} can be calculated by

$$\tau_{o_i} = -c_i(t)\big(M_o\ddot{X}_o + C_o\dot{X}_o + G_o\big). \tag{21}$$

Then, the force F_{e_i} exerted on end effector by the target object in (9) can be given as

$$F_{e_i} = F_{ce_i} = \tau_{\text{int}} - c_i(t)\big(M_o\ddot{X}_o + C_o\dot{X}_o + G_o\big). \tag{22}$$

Summarizing the results above, the objective of the cooperation and coordination transportation for the decoupling NMMs can be concluded as follows.

1) *Task Space:* For task-space motion, the objective is to design a set of distributed controllers for the end effectors of the NMMs to cooperatively transport the target object from the initial position to the desired position.
2) *Null Space:* For null-space motion, based on ensuring the safe transportation of the task-space end effectors, a set of distributed controllers is designed for the mobile bases to perform obstacle avoidance task while transporting the target object along the reference path.

III. Path Planning by Modified Virtual Structure

This section uses a modified virtual structure method. The cooperation and coordination transportation for the decoupling NMMs is simplified as an independent synchronization tracking task for task-space end-effectors and null-space mobile bases. The basic idea of the modified virtual structure approach is first formulated, which is then extended as a dynamic one by using the transformation matrix. Moreover, a novel updating law of the path parameter in virtual structure is designed.

A. Concept of Virtual Structure

The virtual structure approach aims to define a virtual reference object (VRO), which represents the center of the desired virtual structure, and the other virtual robots are located on the node of the virtual structure. When the VRO moves along a predefined "baseline" path, a group of reference paths for the actual robots can be obtained by the following equation [27]:

$$\Gamma_i(\sigma_i) = \begin{bmatrix} X_{r0} + R_F^I(\varphi_{ri})l_i(x_{ri}(\sigma_i), y_{ri}(\sigma_i)) \\ \arctan\big(y_{ri}^{\sigma_i}(\sigma_i)/x_{ri}^{\sigma_i}(\sigma_i)\big) \end{bmatrix} \tag{23}$$

where σ_i is the path parameter of the reference path Γ_i. $X_{r0}(\sigma_0) = (x_{r0}(\sigma_0), y_{r0}(\sigma_0))$ is the position of the VRO on the baseline "$\Gamma_0(\sigma_0)$." φ_{ri} denotes the angle between the VRO forward direction and the inertial frame. l_i is the offset vector from the VRO to the node of virtual structure. $R_F^I(\varphi_{ri})$ is the rotation matrix from the Frenet–Serret frame to the inertial frame. Apparently, a desired virtual structure will be established on the condition that all path parameters for reference paths are synchronized. The control goal is then converted to drive the actual robot to track the virtual one. Thus, the cooperative transportation for task-space end-effectors or null-space mobile bases is simplified as a parameter synchronization task and a path tracking task, given as.

1) Parameter Synchronization Task: To enable all path parameters $\sigma_i(t)$ are synchronized to ensure a rigid virtual formation structure, such that

$$\lim_{t\to\infty}\big|\sigma_i(t) - \sigma_j(t)\big| = 0. \tag{24}$$

2) Path Following Task: To enable that the actual structure converges to the virtual one while the position and velocity synchronization between the actual and the virtual structure is achieved, i.e.,

$$\lim_{t\to\infty}\|x_i(t) - x_{ri}(t)\| = 0 \tag{25}$$

where x_i and x_{ri} are, respectively, the state and reference state of NMM i, which includes the position and velocity information.

In some unstructured workspaces, obstacles located at the forward path of the NMMs. Therefore, based on ensuring safe transportation, a dynamic virtual structure needs to be considered. The realization of dynamic virtual structure is achieved based on (23) and the following transformation matrix, given as:

$$\Upsilon = \text{diag}\{\Upsilon_{11},\ \Upsilon_{22}\} \text{ with } \Upsilon_{ii} = \alpha(1-\beta t/L),\ i = 1, 2 \tag{26}$$

where α and β are the transformation factors. L is the step size required to complete the formation transformation. According to the analysis proposed above, a set of dynamic reference paths for actual formation of mobile bases can be generated by (23) and (26).

Remark 1: Different from the virtual structure designed in [23], the path synchronization task in this work not only requires the robot to follow the position of the reference robot but also requires the velocity between the reference robot and the actual robot to be synchronized. This is a more challenging and complex problem compared with [23], only requiring the velocity of robots to be synchronized. In this article, we realize the synchronization of the position and velocity of the actual robot and the virtual robot by using the designed path parameter.

B. Designing of the Path Parameter Updating Law

Based on the above analysis, a synchronous tracking controller is designed for end effectors or mobile bases to achieve cooperation and coordination transportation. The NMMs use path following control to track the reference path. Notice that the path parameters of the reference paths require synchronization. From (23), the reference path $\Gamma_i(\sigma_i)$ is parameterized with path parameter σ_i. Here, an interactive updating rule

Authorized licensed use limited to: b-on: Universidade de Lisboa Reitoria. Downloaded on October 20,2024 at 11:23:04 UTC from IEEE Xplore. Restrictions apply.

is designed to achieve the compromise motion between the virtual structure and the actual one, which is defined as

$$\sigma_i(k+1) = f(\sigma_i(k), \Delta\ell_i) \tag{27}$$

where f is depended on the state error $\Delta\ell_i$ between the actual robot and reference one and the last sampling value of σ_i. For simplicity, f is defined as $f(\cdot) = \sigma_i(k) + \gamma_i Z_i \Delta\ell_i$. γ_i is used to regulate the magnitude of the path parameter. Z_i is an adjustable weight matrix.

Remark 2: It should be noted that (27) is an iterative form of the updating law of path parameters. When $\Delta\ell_i = 0$, that is, the velocity and position of the actual robot and the virtual robot are synchronized, the path parameters will not be updated. Therefore, we assume that the path parameters only use the virtual robot's reference information to update itself.

Remark 3: The state error, including position and velocity, is used to update the path parameter in this work. By introducing the parameter synchronization constraint (24) into the objective function, we can achieve synchronization between different path parameters and then achieve synchronization control between the position and speed of the robots. Compared with path parameter updating the law in [23], and [27], the updating law (27) is more applicable to general situations with less conservative.

IV. Distributed Cooperation and Coordination Control

In this section, the synchronization tracking controllers for the decoupling NMMs with the feasible state and control constraints are designed via the distributed MPC approach. Based on the previous analysis, the task-space end-effectors and null-space mobile bases can be employed to implement different tasks.

One can describe a general discrete state-space form of the decoupled dynamics (11) and (15) with sampling period T as follows:

$$x_i(k+1) = h_i x_i(k) + p_i u_i(k) \tag{28}$$

where $x_i(k) \in \mathcal{X}_i$ and $u_i(k) \in \mathcal{U}_i$ are, respectively, the state vector and input vector. For task-space motion, $x_i = [X_{m_i},\ \dot{X}_{m_i}]^T$, $u_i = u_{m_i}$. For null-space motion, $x_i = [X_{b_i},\ \dot{X}_{b_i}]^T$, $u_i = u_{n_{bi}}$. h_i and p_i are coefficient matrices obtained by (11) and (15). $\mathcal{X}_i$ and $\mathcal{U}_i$ denote the state compact sets and the input compact sets containing its internal origin, respectively. Notably, the system constraints' sets are defined according to the physical constraints and inherent mechanical structural.

Under the framework of decoupling dynamics, by using the modified virtual structure method, the cooperation and coordination transportation is simplified as a synchronization tracking control task for task-space end-effectors and null-space mobile bases, which includes two parts: 1) parameter synchronization and 2) path following tasks. Distributed MPC is a popular and powerful tool for cooperation and coordination control of the multirobot system. In this article, to achieve the goal of the synchronization tracking control for task-space end-effectors and null-space mobile bases, the constraints (24) and (25) are introduced into the cost function J_i, such that

$$\begin{aligned} J_i(k) = &\sum_{l=0}^{M-1} \|\ell_i(k+l|k)\|^2_{Q_i} + \sum_{l=0}^{N-1} \|u_i(k+l|k)\|^2_{R_i} \\ &+ \sum_{l=0}^{M-1} \sum_{j\in\Omega_i} \left\|\sigma_i(k+l|k) - \sigma_j(k+l|k)\right\|^2_{W_{ij}} \\ &+ \|\ell_i(k+M|k)\|^2_{Q_M^i} \end{aligned} \tag{29}$$

where $\ell_i(k+l|k) = x_i(k+l|k) - x_{ri}(k+l|k)$ is the error state vector between the actual state and the reference state of robot i. $e_i(k+l|k)$, $u_i(k+l|k)$, and $\sigma_i(k+l|k)$ are the predicted values of $\ell_i(k)$, $\Delta u_i(k)$, and $\sigma_i(k)$ at time $k+l$ based on the time k, respectively. M and N are the prediciton and control horizon, and $0 \le N \le M$. Q_i and R_i are positive definite weight matrices. The coupling term between the path parameter σ_i and σ_j is the parameter synchronization constraint, and W_{ij} is the adjustable weight matrix. Ω_i represents the set of the neighbor robots for robot i on the fully connected graph. $\ell_i(k+M|k)$ is the state error value at the terminal predicted time $k+M$ based on the time k. Q_M^i is the terminal weighting matrix, which can be obtained by offline calculation to ensure that the system state error can be converged to the rigion where the system is stable. In summary, the synchronization tracking control via distributed MPC approach integrating the path parameter synchronization constraints and system constraints can be described as follows.

Problem 1: Consider the constrained system (28) with the reference path $\Gamma_i(\sigma_i)$, parameter synchronization condition (24), and path following condition (25), the optimal control input vector $\bar{u}_i^*$ can be obtained by solving the following optimization problem:

$$\bar{u}_i^*(k) = \arg \min_{\bar{u}_i(k)} J_i(k) \tag{30}$$

subject to

$$\ell_i(k+l+1|k) = h_i \ell_i(k+l|k) + p_i u_i(k+l|k)$$

$$\ell_i(k|k) = \ell_i(k) \tag{31a}$$

$$\sigma_i(k+l+1|k) = f(\sigma_i(k+l|k), \Delta\ell_i(k+l+1|k)) \tag{31b}$$

$$\ell_i(k+l|k) \in \mathcal{X}_i,\ l = 0,\ \ldots,\ M \tag{31c}$$

$$u_i(k+l|k) \in \mathcal{X}_i,\ l = 0,\ \ldots,\ N \tag{31d}$$

$$\ell_i(k+M|k) \in X_M^i \tag{31e}$$

where X_M^i is the terminal region guaranteeing the system come to be stable.

Remark 4: Problem 1 is a general form for the task- and null-space optimization problem. By solving this problem, we obtain a set of optimal control sequences that can regulate the position of task-space end-effectors or null-space mobile bases to the desired position. From (30), we can observe that the objective function includes different control information of its neighbors. This coupled optimization problem usually optimizes its cost function to obtain control input using the known neighbors' control information. In addition, the design of task-space controllers and null-space controllers is independent of each other.

Authorized licensed use limited to: b-on: Universidade de Lisboa Reitoria. Downloaded on October 20,2024 at 11:23:04 UTC from IEEE Xplore. Restrictions apply.

Denote $\bar{\ell}_i(k+1) = [\ell_i(k+1|k), \ldots, \ell_i(k+M|k)]^T$, $\bar{u}_i(k) = [u_i^T(k|k), \ldots, x_i^T(k+N-1|k)]^T$, $D_{ri}(k+1) = [x_{ri}^T(k+1|k), \ldots, x_{ri}^T(k+M|k)]^T$, the predicted trajectory of the error state is given as follows:

$$\bar{\ell}_i(k+1) = S_{x_i}x_i(k) + S_{u_i}\bar{u}_i(k) - D_{ri}(k+1) \tag{32}$$

where

$$S_{x_i} = \begin{bmatrix} h_i \\ h_i^2 \\ \vdots \\ h_i^M \end{bmatrix}, S_{u_i} = \begin{bmatrix} p_i & 0 & \ldots & 0 \\ h_i p_i & p_i & \ldots & 0 \\ \vdots & \vdots & \vdots & \vdots \\ h_i^M p_i & h_i^{M-1} p_i & \ldots & p_i^{M-N} \end{bmatrix}.$$

Similarly, let $\bar{\sigma}_i(k+1) = [\sigma_i(k+1), \ldots, \sigma_i(k+M)]^T$, the predicted equation of the path parameter σ_i is given as

$$\bar{\sigma}_i(k+1) = S_{\sigma_i}\sigma_i(k) + S_{\ell_i}\bar{\ell}_i(k+1) \tag{33}$$

with

$$S_{\sigma_i} = \begin{bmatrix} I \\ I \\ \vdots \\ I \end{bmatrix}, \; S_{\ell_i} = \begin{bmatrix} \gamma_i Z_i & 0 & \ldots & 0 \\ \gamma_i Z_i & \gamma_i Z_i & \ldots & 0 \\ \vdots & \vdots & \vdots & \vdots \\ \gamma_i Z_i & \gamma_i Z_i & \ldots & \gamma_i Z_i \end{bmatrix}.$$

Substituting (32) and (33) into (29), the cost function (29) can be rewritten as

$$J_i(k) = \left\| S_{x_i}x_i(k) + S_{u_i}\bar{u}_i(k) - D_{ri}(k+1) \right\|_{\bar{Q}_i}^2 + \|\bar{u}_i(k)\|_{\bar{R}_i}^2 + \sum_{l\in\Omega_i} \|\Pi_i \Delta\bar{u}_i(k) + \Xi_{il}\|_{\bar{W}_{ij}}^2 \tag{34}$$

where $\Pi_i = S_{\ell_i}S_{u_i}$, $\Xi_{ij} = S_{\sigma_i}(\sigma_i(k) - \sigma_j(k)) + S_{\ell_i}(S_{x_i}x_i(k) - D_{ri}(k+1)) - S_{\ell_j}(S_{x_j}x_j(k) + S_{u_j}\bar{u}_j(k) - D_{rj}(k+1))$. $\bar{Q}_i$, $\bar{R}_i$, and $\bar{W}_{ij}$ are the extended form of Q_i, R_i, and W_{ij}.

Since the NMMs are limited by the physical constraints and inherent mechanical structure, and the input torque is restricted, which means the input and state constraints need to be considered. In this article, combined with the reference state information x_{ri} obtained by the reference path $\Gamma_i(\sigma_i)$, the state constraint is converged as the error state constraints. Define the lower and upper bounds of the error state and input vector as $\bar{u}_{i\min}$, $\bar{\ell}_{i\min}$, and $\bar{u}_{i\max}$, $\bar{\ell}_{i\max}$, respectively, the input and error state constraints can be described as follows:

$$\bar{u}_{i\min} \le \bar{u}_i(k) \le \bar{u}_{i\max} \tag{35}$$

$$\bar{\ell}_{i\min} \le S_{x_i}x_i(k) + S_{u_i}\bar{u}_i(k) - D_{ri}(k+1) \le \bar{\ell}_{i\max}. \tag{36}$$

Moreover, taking (34)–(36) into consideration, Problem 1 is redescribed as a QP problem, given as follows.

Problem 2: Consider system (28) with the cost function (34), and system constraints (35) and (36), the optimal control input sequences $\bar{u}_i^*(k)$ can be obtained by solving the following QP problem:

$$\bar{u}_i^*(k) = \arg\min_{\bar{u}_i(k)} \left\{ \frac{1}{2}\bar{u}_i^T(k)B_i\bar{u}_i(k) + c_i^T\bar{u}_i(k) \right\} \tag{37}$$

$$\text{s.t.} \;\; l_i \le A_i\bar{u}_i(k) \le h_i \tag{38}$$

where $c_i = 2(S_{u_i}^T\bar{Q}_i(S_{x_i}x_i(k) - D_{ri}(k+1)) + \sum_{j\in\Omega_i}\Pi_i^T\bar{W}_{ij}\Xi_{ij})$, $B_i = 2(S_{u_i}^T\bar{Q}_iS_{u_i} + \bar{R}_i + \sum_{j\in\Omega_i}\Pi_i^T\bar{W}_{ij}\Pi_i)$, $h_i = [\eta_i^T \; \bar{u}_{i\max}^T]^T$, $A_i = [-\bar{I}^T, \; \bar{I}^T, \; -S_{u_i}^T, \; S_{u_i}^T, \; \bar{I}^T]^T$, $\eta_i = [-\bar{u}_{i\min}^T, \; \bar{u}_{i\max}^T, \; \eta_{i\min}, \; \eta_{i\max}]^T$, $l_i = [-\infty \; \bar{u}_{i\min}^T]^T$, $\eta_{i\min} = (-\bar{\ell}_{i\min} - D_{ri}(k+1) + S_{x_i}x_i(k))^T$, $\eta_{i\max} = (\bar{\ell}_{i\max} + D_{ri}(k+1) - S_{x_i}x_i(k))^T$.

Remark 5: Notice that Problem 2 is an equivalent form of Problem 1, and both of them are convex optimization problem for NMMs. As the null-space optimization variable $\bar{u}_i(k)$ contains the auxiliary control input $u_{\theta_{b_i}}$, the constraints (35) and (36) or (38) cannot directly be employed to the optimization problem (37). Therefore, those constraints applied to $u_{\theta_{b_i}}$ must be expressed in terms of $\bar{u}_i(k)$ through the nonlinear mapping $\tau_{n_{b_i}} = B_{\theta_{b_i}}^{-1}(M_{\theta_{b_i}}u_{\theta_{b_i}} + C_{\theta_{b_i}}\dot{\theta}_{b_i})$ between the null-space physical input $\tau_{n_{b_i}}$ and the auxiliary control input $u_{\theta_{b_i}}$.

Remark 6: In problem 2, the desired information D_{ri} is utilized to obtain the optimal control input $\bar{u}_i^*$. However, according to the predicted equation of the path parameter (33), when the prediction horizon $M > 1$, we cannot obtain the predicted value of the path parameter via the actual robot state because only the current actual state can be obtained at each sampling time instant. In this work, the predicted state value of the robot i is used to update the path parameter and obtain the predicted path parameter. In this way, the initial parameter synchronization error will be larger than directly using the real state to predict the path parameters. However, when the predicted state of the system finally converges to the desired system state, the two methods are equivalent.

V. Distributed Neurodynamics Optimization and Stability Analysis

In this section, a GPNN online optimization approach is first employed to solve Problem 2 to obtain an optimal solution $\bar{u}_i^*$. The stability analysis of the system is then reported. To start with, the dynamic equation of GPNN is written as follows [30]:

$$\varphi\vartheta^+\Lambda + \rho = K_\Lambda\left(\rho - \vartheta^+\Lambda + \varphi\vartheta^+\Lambda\right) \tag{39}$$

with $\zeta = -B_i^{-1}c_i$, $\Lambda = \bar{u}_i(k) - \zeta$, $\varphi = A_i^TB_iA_i$, $\rho = -A_iB_i^{-1}c_i$, $\vartheta = B_i^{-1}A_i^T$, and ϑ^+ denotes the pseudoinverse of ϑ. K_Λ represents the projection operator, which is defined as

$$K_\Lambda = \begin{cases} l_i, & \bar{u}(k)_i < l_i \\ \bar{u}_i(k), & \bar{u}_i(k) \in [l_i, \; h_i] \\ h_i, & \bar{u}_i(k) > h. \end{cases} \tag{40}$$

Denote $\lambda = \vartheta$, $\Im(\Delta\bar{u}_i(k)) = \vartheta^+\Lambda$, and $\aleph(\bar{u}_i(k)) = \varphi\mu\vartheta^+\Lambda + \rho$, the neural dynamic equation of the GPNN is shown as follows:

$$\gamma\frac{d\bar{u}_i(k)}{dt} = \lambda[K_\Lambda(\aleph(\bar{u}_i(k)) - \Im(\bar{u}_i(k))) - \aleph(\Delta\bar{u}_i(k))] \tag{41}$$

and $\bar{u}_i(k)$ is defined as the neural network state vector, and γ is a positive constant. For more details of the structure of GPNN, readers can be refer to [29]. Notice that GPNN (41) is a discontinuous-time dynamic equation, and its implementation is achieved by using the MATLAB Simulink toolbox in this article. By solving the neural dynamic equation repeatedly, we can obtain a convergent optimal control input increment $\bar{u}_i^*(k)$. The analysis of the global exponential convergence of the GPNN can be referred to [31]. Before giving the analysis of the closed-loop system stability, we first introduce the following assumption and lemma.

Authorized licensed use limited to: b-on: Universidade de Lisboa Reitoria. Downloaded on October 20,2024 at 11:23:04 UTC from IEEE Xplore. Restrictions apply.

Assumption 1: Since MPC is a method that uses finite horizon optimization to approximate the solution of ininite time-domain optimal control. For system (28) and cost function (29), if the prediction step is larger than M, the prediction control input vector $u_i(k+j|k)$ is defined as follows:

$$u_i(k+l|k) = \kappa_i(x_i(k+l|k) - x_{ri}(k+l|k)),\ l \geq M \quad (42)$$

where κ_i is the feedback gain, and $u_i(k+l|k) \in \mathcal{U}_i$ for any $l \geq M$.

Lemma 1 [36]: For system (28), given positive symmetric matrices $Q_i > 0$ and $R_i > 0$, there exist a positive definite symmetric matrix Q_M^i, a state feedback control law κ_i, such that: 1) $\forall \ell_i \in \mathcal{X}_i$, $\kappa_i \ell_i \in \mathcal{U}_i$, and $\|(h_i + p_i\kappa_i)\ell_i\|^2_{Q_M^i} - \|\ell_i\|^2_{Q_M^i} \leq -\|\ell_i\|^2_{Q_i} - \|\kappa_i\ell_i\|^2_{R_i}$, where $X_M^i = \{\ell_i \in R^n | \ell_i^T Q_M^i \ell_i \leq 1\}$ and 2) $\forall \ell_i \in \mathcal{X}_i$, $(h_i + p_i\kappa_i)\ell_i \in \mathcal{X}_i$.

Based on Lemma 1 and Assumption 1, the following theorem is given to guarantee the stability of the closed-loop system by using the GPNN-based distributed MPC controller.

Theorem 1: For system (28) with performance index (29), if the path parameter error between NMM i and its neighboring NMM i satisfies the following condition:

$$\left\|\sigma_i^*(k+l|k) - \sigma_j^*(k+l|k)\right\|_{W_{ij}} \leq \sqrt{\frac{\lambda_{\min}(F_i)}{(L-1)\lambda_{\max}\left(Q_M^i\right)}} \quad (43)$$

where $l \geq M$, L is the number of NMMs. $\lambda_{\min}(F_i)$ and $\lambda_{\max}(F_i)$ represent the minimum eigenvalue and maximun eigenvalue of matrix F_i, $F_i = Q_M^i - Q_i - \kappa_i^T R_i \kappa_i - (h_i + p_i\kappa_i)^T Q_M^i (h_i + p_i\kappa_i)$, then, the cost function satisfies $\Delta J \leq 0$, and the closed-loop system converges to the terminal region $X_M^i = \{\ell_i \in R^n | \ell_i^T Q_M^i . \ell_i \leq 1\}$ by using the GPNN-based distributed MPC strategy.

Proof: According to the Lemma 1, the optimal control and error state sequences can be obtained. We denote the corresponding sequences satisfying system input and error state constraints as $\bar{u}_i^*(k) = [u_i^{*T}(k|k), \ldots, u_i^{*T}(k+M-1|k)]^T$, and $\bar{\ell}_i^*(k) = [\ell_{ei}^{*T}(k+1|k), \ldots, \ell_{ei}^{*T}(k+M-1|k)]^T$. Moreover, the optimal cost function is given as

$$\begin{aligned}\Phi(k) = &\left\|\ell_i^*(k+M|k)\right\|^2_{Q_M^i} \\ &+ \sum_{l=0}^{M-1}\Bigg[\left\|\ell_i^*(k+l|k)\right\|^2_{Q_i} + \left\|u_i^*(k+l|k)\right\|^2_{R_i} \\ &+ \sum_{j\in\Omega_i}\left\|\sigma_i^*(k+l|k) - \sigma_j^*(k+l|k)\right\|^2_{W_{ij}}\Bigg]. \end{aligned} \quad (44)$$

Obviously, for $\forall\ \ell_i(k) \neq 0$, $\Phi(\ell_i(k)) > 0$ is continuous as $\ell_i(k) = 0$. Then, at time $k+1$, the distributed cost function can be expressed as follows:

$$\begin{aligned}&J_i(k+1) \\ &= \|\ell_i(k+M+1|k+1)\|^2_{Q_M^i} \\ &\quad + \sum_{l=0}^{M-1}\Bigg[\|\ell_i(k+l+1|k+1)\|^2_{Q_i} + \|u_i(k+l+1|k+1)\|^2_{R_i} \\ &\quad + \sum_{j\in\Omega_i}\left\|\sigma_i(k+l+1|k+1) - \sigma_j(k+l+1|k+1)\right\|^2_{W_{ij}}\Bigg]. \end{aligned} \quad (45)$$

According to the principle of optimality, for $l = 0, 1, \ldots, M$, $\ell_i^*(k+l+1|k) - \ell_i(k+l+1|k+1) \to 0$, $\sigma_i^*(k+l+1|k) - \sigma_i(k+l+1|k+1) \to 0$, and $u_i^*(k+l+1|k) - u_i(k+l+1|k+1) \to 0$. Hence, the following inequality can be obtained:

$$\begin{aligned}J_i(k+1) = &\sum_{l=0}^{M-1}\Bigg[\left\|\ell_i^*(k+l+1|k)\right\|^2_{Q_i} + \left\|u_i^*(k+l+1|k)\right\|^2_{R_i} \\ &+ \sum_{j\in\Omega_i}\left\|\sigma_i^*(k+l+1|k) - \sigma_j^*(k+l+1|k)\right\|^2_{W_{ij}}\Bigg] \\ &+ \left\|\ell_i^*(k+M+1|k)\right\|^2_{Q_M^i} \\ \leq\ &\Phi(k) - \left\|\ell_i^*(k|k)\right\|^2_{Q_i} - \left\|u_i^*(k|k)\right\|^2_{R_i} + \Theta_{iN} \\ &- \sum_{j\in\Omega_i}\left\|\sigma_i^*(k|k) - \sigma_j^*(k|k)\right\|^2_{W_{ij}} \end{aligned} \quad (46)$$

and the terminal item is given as

$$\begin{aligned}\Theta_{iN} = &\left\|\ell_i^*(k+M|k)\right\|^2_{Q_i} + \left\|u_i^*(k+M|k)\right\|^2_{R_i} \\ &+ \left\|\ell_i^*(k+M+1|k)\right\|^2_{Q_M^i} - \left\|\ell_i^*(k+M|k)\right\|^2_{Q_M^i} \\ &+ \sum_{j\in\Omega_i}\left\|\sigma_i^*(k+M|k) - \sigma_j^*(k+M|k)\right\|^2_{W_{ij}}. \end{aligned} \quad (47)$$

From (46) and (47), the following relationship is established:

$$\begin{aligned}\Phi(k+1) &\leq \Phi(k) - \left\|\ell_i^*(k|k)\right\|^2_{Q_i} - \left\|u_i^*(k|k)\right\|^2_{Q_i} \\ &\leq -\sum_{j\in\Omega_i}\left\|\sigma_i^*(k|k) - \sigma_j^*(k|k)\right\|^2_{W_{ij}} + \Theta_{iN}. \end{aligned} \quad (48)$$

Next, we prove that $\Theta_{iN} \leq 0$. According to [35] and condition (43), we have

$$\begin{aligned}\Theta_{iN} &\leq \frac{\lambda_{\min}(-F_i)}{\lambda_{\max}\left(Q_M^i\right)}\left\|\ell_i^*(k+M|k)\right\|^2_{Q_M^i} \\ &\quad + \sum_{j\in\Omega_i}\left\|\sigma_i^*(k+M|k) - \sigma_j^*(k+M|k)\right\|^2_{W_{ij}} \\ &\leq 0. \end{aligned} \quad (49)$$

Consequently, we can obtain

$$\Phi(k+1) \leq \Phi(k) - \left\|\ell_i^*(k|k)\right\|^2_{Q_i}. \quad (50)$$

Clearly, the equation holds if and only if $\ell_i^* = 0$ and $u_i^* = 0$. The above analysis shows that $\Phi(k)$ will converge to the terminal region X_M^i along the system's trajectory, that is, the closed-loop system is asymptotically stable. ■

Ultimately, the algorithm of the GPNN-based distributed MPC strategy for the decoupling NMMs is summarized as follows.

VI. Simulations

In this section, two simulation examples are given to demonstrate the effectiveness of the proposed cooperation and coordination transportation strategy for the decoupling NMMs. In Example A, the reference trajectory is first given, and the classical consensus control strategy in [20] is considered and compared with our proposed GPNN-based distributed

Authorized licensed use limited to: b-on: Universidade de Lisboa Reitoria. Downloaded on October 20,2024 at 11:23:04 UTC from IEEE Xplore. Restrictions apply.

Algorithm 1 Proposed GPNN-Based Distributed MPC Algorithm

1: Initialization: At $k = 0$, initialize the virtual structure parameters: $\Gamma_0(\sigma_0)$, σ_i, l_i, DMPC parameters: M, N, R_i, Q_i, the initial state of NMMs, the sampling period T, and other related parameters;
2: Reference path generation: For NMM i, its reference path is obtained by (23);
3: Communication: NMM i sends its position and velocity information to its neighbor robots by using Wi-Fi, and receiving its neighbors' information;
4: Optimization preparation: For NMM i, establish the constrained QP problem and calculate the following matrices in (37)-(38): B_i, c_i, A_i, l_i, and h_i;
5: Local optimization: To obtain the optimal solution of system (28), the neurodynamic equation (41) is employed to solve the constrained QP problem (37)-(38);
6: Path updating: Based on the results of step 5, the position and velocity information of NMM i is updated by (27);
7: Receding horizon: Let $k = k+1$, go to step 2 if the NMMs keep moving on.

MPC strategy. Moreover, the performance of the disturbances avoidance for the two strategies is also considered. In Example B, with the fixed obstacles, a cooperation and coordination transportation problem is solved by the modified virtual structure and the GPNN-based distributed MPC strategy given in Algorithm 1. For simplicity, three NMMs are controlled to implement the cooperation and coordination transportation task by grasping different points of the target object. All physical parameters of NMMs are assumed to be identical and can refer to [33]. The communication topology is selected as a fully connected graph.

Example A (General Transportation Example With Compared Results): In this example, a general transportation example with given reference trajectory is considered for the decoupling NMMs, and the classical consensus control strategy in [20] is compared with our proposed GPNN-based distributed MPC strategy. The reference trajectory for the target object, end-effectors, and mobile bases is defined as $X_{ro} = [0.2 + 0.2t,\ 0.1 + \sin(t/100)]^T$, $X_{rm1} = X_{ro} + [1/2\sqrt{3},\ 0.5]^T$, $X_{rm2} = X_{ro} + [-1/\sqrt{3},\ 0]^T$, $X_{rm3} = X_{ro} + [1/2\sqrt{3},\ -0.5]^T$, $X_{rb1} = X_{ro} + [1/2\sqrt{3},\ 1.1]^T$, $X_{rb2} = X_{ro}+[1/2\sqrt{3}+0.9,\ 0]^T$, $X_{rb3} = X_{ro}+[1/2\sqrt{3},\ -1.1]^T$. The sampling period T is taken as 0.1 s. Since these reference trajectories are twice differentiable, the reference velocities for the target object, end-effectors, and mobile bases can be calculated directly. The initial states for end-effectors and mobile bases of the NMMs are given as: $X_{m1} = [0.5\ 1]^T$, $X_{m2} = [-0.3,\ 0.5]^T$, $X_{m3} = [0.6,\ -0.8]^T$, $X_{b1} = [0.3,\ 1.5]^T$, $X_{b2} = [0.7,\ -0.3]^T$, and $X_{b3} = [0.72,\ -1.2]^T$. All velocities of end-effectors and mobile bases are initialized as zeros. The parameters of the consensus control are set same as [20]. The prediction and control horizons are set as: $M = 5$ and $N = 1$. The weighted matrices of the distributed MPC are given as: $W_{ij} = 0.1I_{1\times1}, ij \in \Omega_i$, $Q_{mi} = 20I_{4x4}$, $R_{mi} = 0.1I_{2x2}$, $i = 1, 2, 3$. $Q_{bi} = 25I_{4x4}$, $R_{bi} = 0.1I_{2x2}$, $i = 1, 2, 3$. The external disturbance vector is given as $w_{mi} = [0.5\sin(t);\ 0.2\sin(t);\ 0;\ 0]$. The terminal weight matrix in task space and null space is calculated by condition in Lemma 1 and the related parameters. All simulation results are shown as Figs. 1–6, where the dotted line and the label "CNMM i" represent the result obtained by the consensus control, and the dashed line represented by a line segment and the label "DNMM i" represents the results obtained by the algorithm proposed in this article. Besides, we use blue, black, and red to represent NMM1, NMM2, and NMM3.

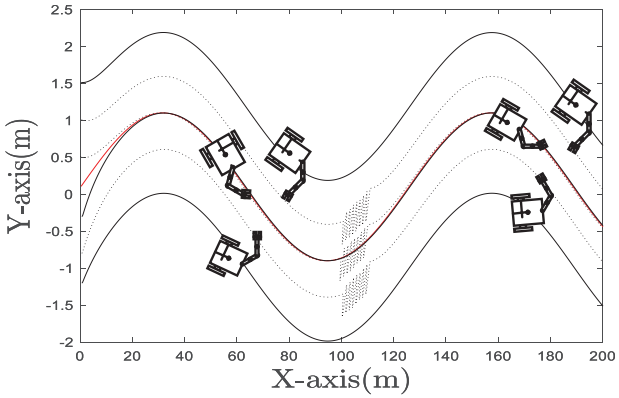

Fig. 1. General transportation trajectory for the NMMs via the GPNN-based distributed MPC strategy.

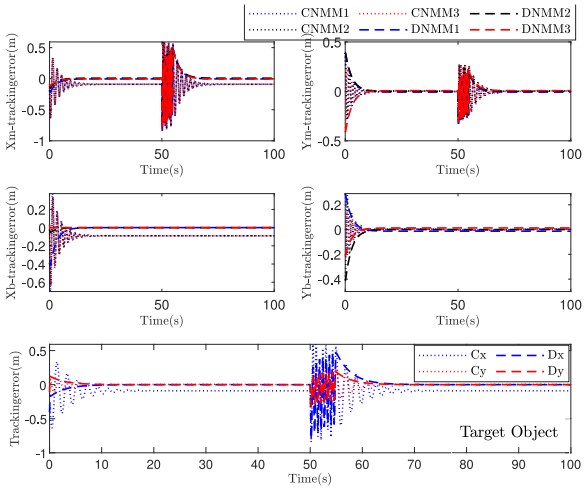

Fig. 2. Tracking errors of the decoupled NMMs and the target object.

The transportation trajectory of the end-effectors and mobile bases of the NMMs are shown in Fig. 1, where the solid red line is the trajectory of the target object, the black dotted line is the trajectories of the end effectors, and the solid black line is the trajectories of the mobile bases. From Fig. 1, we can see that the decoupling NMMs keep the desired structure and move along the reference trajectories, which means cooperation and coordination transportation for the decoupling NMMs can be achieved. The tracking errors and velocity errors are shown in Figs. 2 and 3. It can be seen that the tracking errors and velocity errors for end-effectors and mobile bases of NMMs obtained by the consensus control strategy oscillate

Authorized licensed use limited to: b-on: Universidade de Lisboa Reitoria. Downloaded on October 20,2024 at 11:23:04 UTC from IEEE Xplore. Restrictions apply.

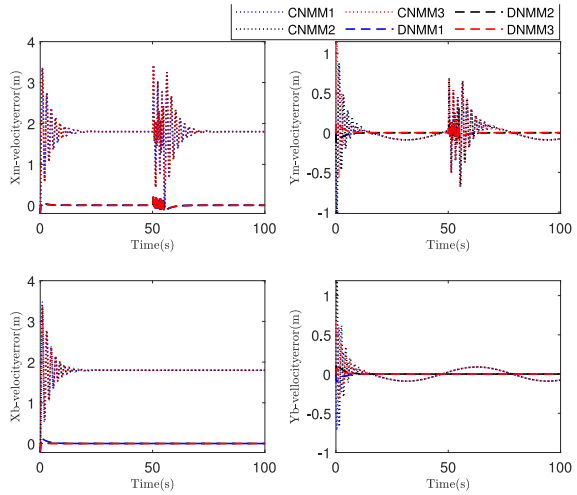

Fig. 3. Velocity errors of the decoupled NMMs and the target object.

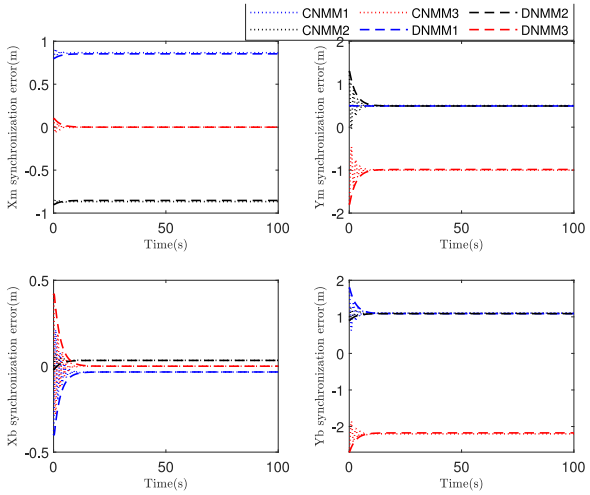

Fig. 4. Position errors between neighboring robots on the communication topology graph of the decoupled NMMs.

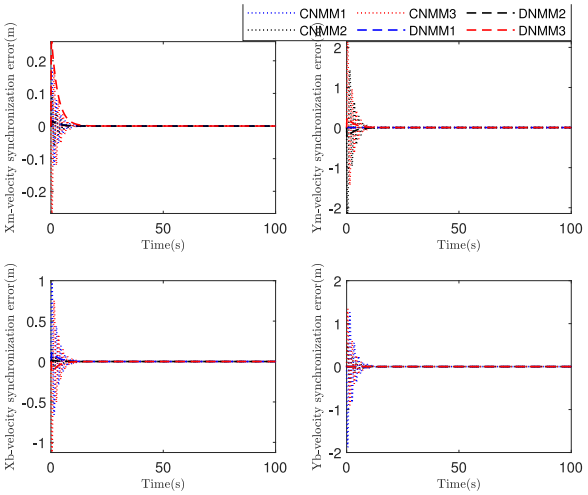

Fig. 5. Velocity errors between neighboring robots on the communication topology graph of the decoupled NMMs.

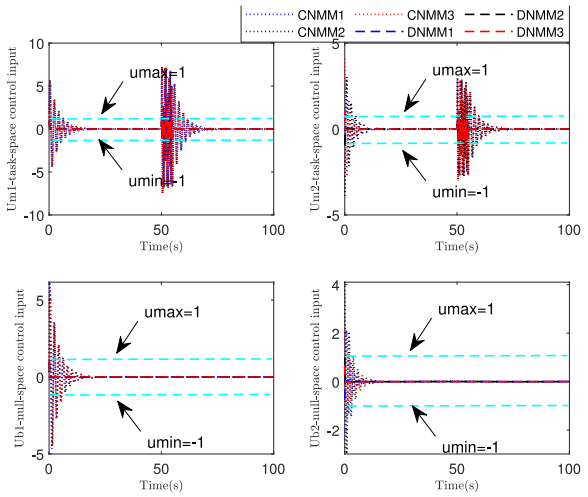

Fig. 6. Control input of the decoupled NMMs.

and converge to a stable value instead of zero in the first 15 s. Furthermore, from Figs. 4 and 5, we can find that the position and velocity errors between neighboring robots on the communication topology graph can converge to the expectations faster. According to the above analysis, we can conclude that although NMMs can achieve cooperative and coordinative transportation via the consensus control method in [20], the positions and velocities for end-effectors and mobile bases cannot perfectly meet the set expectations. Moreover, it can be observed from Figs. 2–5 that the tracking errors, velocity errors, and the position and velocity errors between neighboring robots on the communication topology graph for the end-effectors and mobile bases of NMMs can quickly and compliantly converge to zeros via the proposed GPNN-based distributed MPC strategy, which means that our proposed strategy can better accomplish coordinated and cooperative transportation tasks for the decoupling NMMs. To verify the performance of the two strategies in the presence of disturbances, we applied the disturbances to the target object between 50 and 55 s. From Figs. 2 and 3, we can see that both strategies can stabilize the task-space system consisting of the end effectors. However, the system's degree of oscillation and convergence time under the action of consensus control is much longer than those under the control strategy proposed in this article. This fact reveals that the system has good robustness via the proposed GPNN-based distributed MPC strategy. In Fig. 6, the upper and lower bounds of the control inputs are set as $u_max = 1$ and $u_min = -1$ labeled by the cyan-dotted line. It can be observed from Fig. 6 that the control input of our proposed distributed MPC strategy is lower than the consensus control strategy. It always satisfies the control input constraint, especially during the period when the system is disturbed. Summarizing the discussion above, we can conclude that: compared with the consensus control strategy in [20], our proposed GPNN-based distributed MPC strategy can always ensure that the system control input and state are always within the feasible constraint range, synchronize the position and velocity of NMMs, and has better performance and robustness.

Authorized licensed use limited to: b-on: Universidade de Lisboa Reitoria. Downloaded on October 20,2024 at 11:23:04 UTC from IEEE Xplore. Restrictions apply.

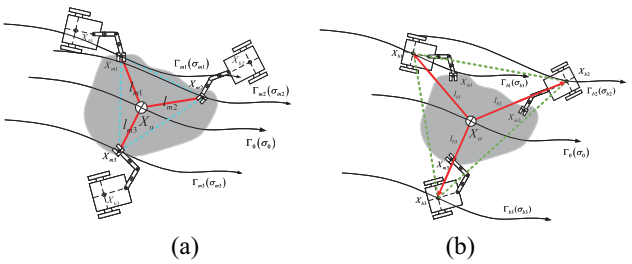

Fig. 7. Illustration of the virtual structure for the decoupling NMMs. (a) Rigid structure for task-space end effectors, where the cyan-dotted triangle is the desired rigid virtual structure, X_o denotes the center of the virtual structure, $\Gamma_{mi}(\sigma_{mi})$ is the reference path, and $l_{mi}(i = 1, 2, 3)$ represents the offset vector of the virtual structure. (b) Dynamic virtual structure for null-space mobile bases, where the virtual structure, reference path $\Gamma_{bi}(\sigma_{bi})$, and offset vector are defined similar as (a), and the dynamic virtual structure is achieved by (26).

Case B (Cooperation and Coordination Transportation Example With the Obstacles): In this example, a cooperation and coordination transportation example with the obstacles is considered and solved by the modified virtual structure, and the GPNN-based distributed MPC strategy given in Algorithm 1. For simplicity, we only consider the fixed obstacles.

Here, two virtual structures are, respectively, defined for task-space end-effectors and null-space mobile bases and shown in Fig. 7(a) and (b), where a rigid virtual structure is defined for task-space end-effectors ensuring the safe and stable transportation. A dynamic virtual structure is defined for null-space mobile bases to avoid obstacles; meanwhile, switch the motion path of the target object to reach the desired position. The base line of the virtual structure (i.e., the reference path of the target object) is defined as the multisegment line, given as: $\Gamma_0(\sigma_0) = [0.2\sigma_0(t) + 0.2,\ 0.1]^T$ m at $0 \le \sigma_0 \prec 30$; $\Gamma_0(\sigma_0) = [0.2\sigma_0(t) + 0.2,\ 0.07(\sigma_0(t) - 30) + 0.1]^T$ m at $30 \le \sigma_0 \prec 40$; $\Gamma_0(\sigma_0) = [0.2\sigma_0(t) + 0.2; 0.8]^T$ m at $\sigma_0 \ge 40$. The task-space offset vectors are given as $l_{m1} = [0.29,\ 0.5]^T$, $l_{m2} = [-0.28,\ 0]^T$, and $l_{m3} = [0.29,\ -0.7]^T$. The null-space offset vectors are given as $l_{b1} = [0.29,\ 1.2]^T$, $l_{b2} = [0.32,\ 0.3]^T$, and $l_{b3} = [0.29,\ -0.6]^T$. The description of the dynamic virtual structure for the decoupled mobile bases has been given in Section III, and the transformation parameters in (27) are set as: $\alpha_1 = 1$, $\alpha_2 = 1$, $\beta = 0.1$, and $L = 10$. This setting aims to achieve a 10% decrement from the initial formation structure when the team encounters obstacles. The initial states for end-effectors and mobile bases of the NMMs are given as: $X_{m1} = [1.29,\ 0.8\ 0.2\ 0]$, $X_{m2} = [-0.02,\ 0.2\ 0.2\ 0]$, $X_{m3} = [0.49,\ -0.45\ 0.2\ 0]$, $X_{b1} = [0.55,\ 1.5\ 0.2\ 0]$, $X_{b2} = [0.76,\ 0.3\ 0.2\ 0]$, and $X_{b3} = [0.65,\ -0.8\ 0.2\ 0]$. The initial value of the path parameters for task-space and null-space motion is given as: $\sigma_{m1} = 4$, $\sigma_{m2} = 2$, $\sigma_{m3} = 0$, $\sigma_{b1} = 0.52$, $\sigma_{b2} = 1.2$, and $\sigma_{b3} = 0.5$. The prediction and control horizons are set as: $M = 5$ and $N = 1$. The weighted matrices of the distributed MPC are given same as Example A. All simulation results are shown in Figs. 8–13.

The transportation paths of the end-effectors and mobile bases of the NMMs are shown in Fig. 8, where the two black

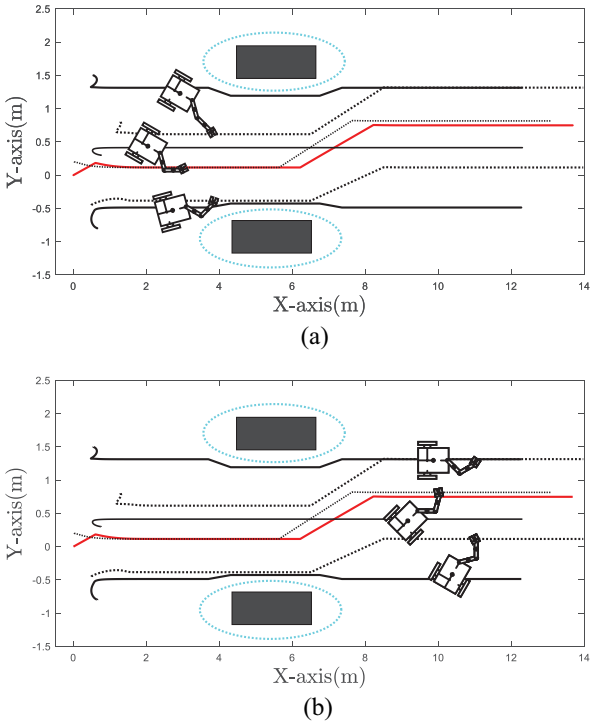

Fig. 8. Cooperation and coordination transportation with obstacles for NMMs. (a) Time = 50 s. (b) Time = 150 s.

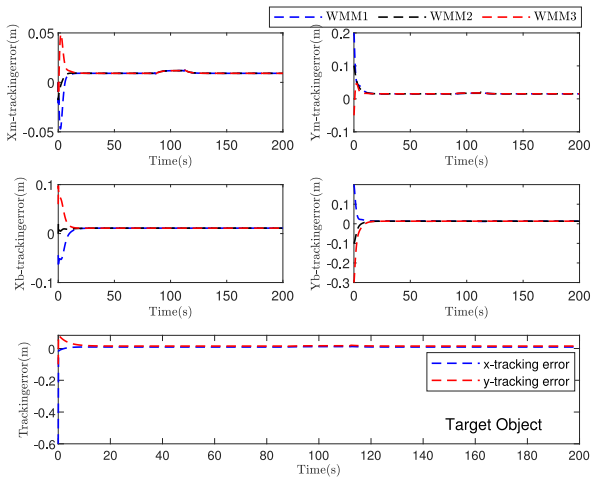

Fig. 9. Tracking errors of the decoupled NMMs and the target object.

rectangles denote the obstacles existing on the forward path. It can be seen from Fig. 8 that: the NMMs can regulate the positions of mobile bases to avoid obstacles while transporting the target object to the desired location. Meanwhile, the end-effectors can maintain a rigid structure to transport the target object and follow the baseline. Notice that the reference paths for the end-effectors are developed with the baseline of the target object, and the reference path of the mobile bases is kept unchanged. The tracking errors of the decoupled NMMs are shown in Fig. 9. Since the end effectors need to switch their path transporting the target object to the desired position, the tracking errors of the end-effectors cannot always converge to be zeros at time 85–115 s. However,

Authorized licensed use limited to: b-on: Universidade de Lisboa Reitoria. Downloaded on October 20,2024 at 11:23:04 UTC from IEEE Xplore. Restrictions apply.

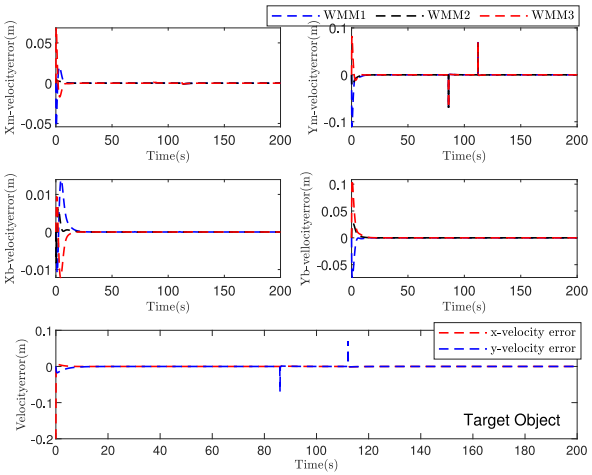

Fig. 10. Velocity errors of the decoupled NMMs and the target object.

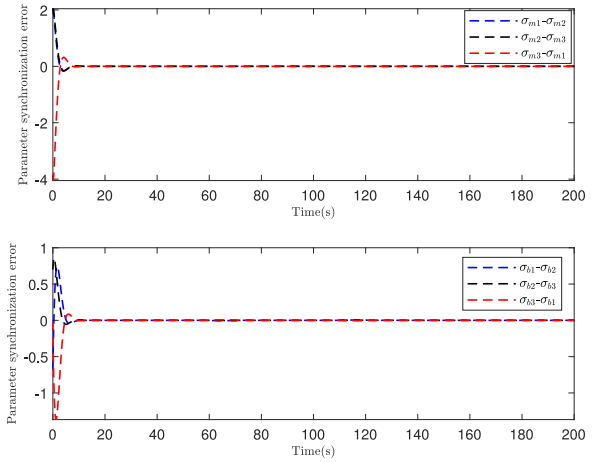

Fig. 11. Path synchronization error of the decoupled NMMs.

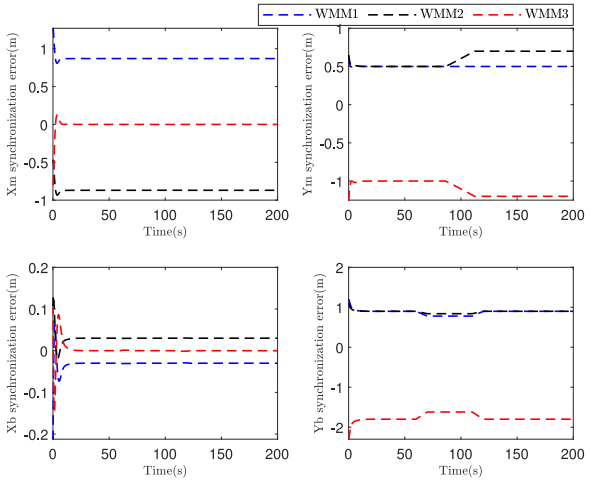

Fig. 12. Position errors between neighboring robots on the communication topology graph of the decoupled NMMs.

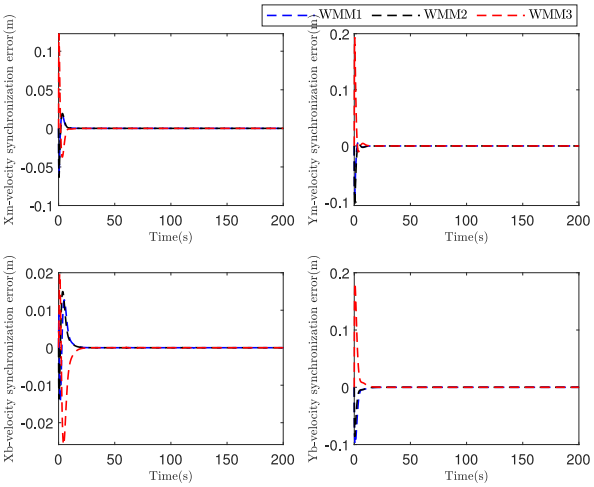

Fig. 13. Velocity errors between neighboring robots on the communication topology graph of the decoupled NMMs.

the target object can be guaranteed to follow the baseline reference path, and the tracking errors of the mobile bases can quickly converge to a stable value near zero. This is because, under the framework of decoupling control, the task-space motion and the null-space motion are independent and complementary to each other. This conclusion can also be supported by Fig. 10, where the velocity fluctuation of the task-space end-effectors does not affect the velocity of the null-space mobile bases. The parameter synchronization error, the position errors, and velocity error between neighboring robots on the communication topology graph of the decoupled NMMs are, respectively, shown in Figs. 11–13. It can be observed that when the parameter synchronization errors tend to zero in 0–10 s, the velocity error between neighboring robots on the communication topology graph of the decoupled NMMs also converges to zero. The position error between adjacent robots converges to the given value of the virtual structure, which means that the decoupling NMMs can quickly achieve synchronization via the proposed GPNN-based distributed MPC strategy. It is worth noting that in Fig. 12, the change in the synchronization position error of the end-effectors in the Y direction is mainly because the end-effectors need to adjust their positions to transport the target object to the desired position, which is consistent with the reference path change of the target object. The position change in the Y direction of the mobile bases is because it needs to adjust its position to avoid obstacles and return to the original reference path. The GPNN-based distributed MPC strategy proposed in this article can effectively solve the coordinated and cooperative transportation problem for the decoupling NMMs.

VII. Conclusion

This article investigates the cooperation and coordination transportation problem of the decoupling NMMs with the feasible state and input constraints. A GPNN-based distributed MPC strategy is proposed to drive the decoupling NMMs to achieve the synchronization tracking control task. The sufficient condition guaranteeing the stability of the closed-loop system is developed. In simulations, we first verify the effectiveness and superiority of the proposed GPNN-based distributed MPC strategy by comparing it with the classical consensus control strategy. Moreover,

Authorized licensed use limited to: b-on: Universidade de Lisboa Reitoria. Downloaded on October 20,2024 at 11:23:04 UTC from IEEE Xplore. Restrictions apply.

a cooperation and coordination transportation example with the obstacles is considered and solved by the modified virtual structure and the GPNN-based distributed MPC approach. These two typical examples reveal the effectiveness of the proposed GPNN-based distributed cooperation and coordination transportation strategy. It is worth mentioning that there are still issues that need to be considered in cooperation and coordination transportation for decoupling NMMs in practical applications, such as model uncertainty, including external disturbances, dynamic obstacle avoidance, and obstacle avoidance between agents. We will consider the above issues to enhance this work in the future.

REFERENCES

[1] M. Deng, Z. Li, Y. Kang, C. L. P. Chen, and X. Chu, "A learning-based hierarchical control scheme for an exoskeleton robot in human-robot cooperative manipulation," *IEEE Trans. Cybern.*, vol. 50, no. 1, pp. 112–125, Jan. 2020.

[2] W. He, Y. Sun, Z. Yan, C. Yang, Z. Li, and O. Kaynak, "Disturbance observer-based neural network control of cooperative multiple manipulators with input saturation," *IEEE Trans. Neural Netw. Learn. Syst.*, vol. 31, no. 5, pp. 1735–1746, May 2020.

[3] B. Sharma, S. Singh, J. Vanualailai, and A. Prasad, "Globally rigid formation of n-link doubly nonholonomic mobile manipulators," *Robot. Auton. Syst.*, vol. 105, pp. 69–84, Jul. 2018.

[4] S. Heshmati-Alamdari, C. P. Bechlioulis, G. C. Karras, and K. J. Kyriakopoulos, "Cooperative impedance control for multiple underwater vehicle manipulator systems under lean communication," *IEEE J. Ocean. Eng.*, vol. 46, no. 2, pp. 447–465, Apr. 2021.

[5] H. J. Savino, L. C. A. Pimenta, J. A. Shah, and B. V. Adorno, "Pose consensus based on dual quaternion algebra with application to decentralized formation control of mobile manipulators," *J. Franklin Inst.*, vol. 357, no. 1, pp. 142–178, 2020.

[6] H. Zhang, Q. Sheng, Y. Sun, X. Sheng, Z. Xiong, and X. Zhu, "A novel coordinated motion planner based on capability map for autonomous mobile manipulator," *Robot. Auton. Syst.*, vol. 129, Jul. 2020, Art. no. 103554.

[7] D. Qin, A. Liu, J. Xu, W.-A. Zhang, and L. Yu, "Learning from human demonstrations for wheel mobile manipulator: An unscented model predictive control approach," *IEEE Trans. Neural Netw. Learn. Syst.*, early access, May 12, 2022, doi: 10.1109/TNNLS.2022.3171595.

[8] H. Xing *et al.*, "An admittance-controlled wheeled mobile manipulator for mobility assistance: Human–robot interaction estimation and redundancy resolution for enhanced force exertion ability," *Mechatronics*, vol. 74, Apr. 2021, Art. no. 102497.

[9] B. Elaamery, M. Pesavento, T. Aldovini, N. Lissandrini, G. Michieletto, and A. Cenedese, "Model predictive control for cooperative transportation with feasibility-aware policy," *Robotics*, vol. 10, no. 3, pp. 1–20, Jun. 2021.

[10] B. Teka and A. Dutta, "Modeling and simulation of cooperative transport of an object by two mobile manipulators on an uneven terrain using KSOM network," *Int. J. Model. Simul.*, vol. 41, no. 1, pp. 39–51, Sep. 2021.

[11] Y. Wang and C. W. de Silva, "Sequential Q-learning with Kalman filtering for multirobot cooperative transportation," *IEEE/ASME Trans. Mechatronics*, vol. 15, no. 2, pp. 261–268, Apr. 2010.

[12] J. Obregón and A. Morales, "Synchronized mobile manipulators for kinematic cooperative tasks: Control design and analysis," *IFAC-PapersOnLine*, vol. 53, no. 2, pp. 9074–9079, 2020.

[13] K. Shojaei, "An adaptive output feedback proportional-integral-derivative controller for n-link type (m, s) electrically driven mobile manipulators," *J. Dyn. Syst. Meas. Control*, vol. 141, no. 9, pp. 2028–2034, Apr. 2019.

[14] Z. Li, J. Li, and Y. Kang, "Adaptive robust coordinated control of multiple mobile manipulators interacting with rigid environments," *Automatica*, vol. 46, no. 12, pp. 2028–2034, Jul. 2010.

[15] M. Rani, N. Kumar, and H. P. Singh, "Motion/force control scheme for electrically driven cooperative multiple mobile manipulators," *Control Eng. Pract.*, vol. 88, pp. 52–64, Jul. 2019.

[16] Y. Ren, S. Sosnowski, and S. Hirche, "Fully distributed cooperation for networked uncertain mobile manipulators," *IEEE Trans. Robot.*, vol. 36, no. 4, pp. 984–1003, Aug. 2020.

[17] C. Wu, H. Fang, Q. Yang, X. Zeng, Y. Wei, and J. Chen, "Distributed cooperative control of redundant mobile manipulators with safety constraints," *IEEE Trans. Cybern.*, early access, Aug. 30, 2021, doi: 10.1109/TCYB.2021.3104044.

[18] Q. Tang, Y. Zhang, F. Yu, and J. Zhang, "An obstacle avoidance approach based on system outlined rectangle for cooperative transportation of multiple mobile manipulators," in *Proc. IEEE Int. Conf. Intell. Safety Robot. (ISR)*, 2018, pp. 533–538, doi: 10.1109/IISR.2018.8535773.

[19] J. Chen and S. Kai, "Cooperative transportation control of multiple mobile manipulators through distributed optimization," *Sci. China Inf. Sci.*, vol. 61, no. 12, pp. 1–17, Dec. 2018.

[20] G.-B. Dai and Y.-C. Liu, "Distributed coordination and cooperation control for networked mobile manipulators," *IEEE Trans. Ind. Electron.*, vol. 64, no. 6, pp. 5065–5074, Jun. 2017.

[21] M. Xue, Y. Tang, W. Ren, and Q. Feng, "Practical output synchronization for asynchronously switched multi-agent systems with adaption to fast-switching perturbations," *Automatica*, vol. 116, pp. 1–12, Jun. 2020.

[22] A. Liu, W.-A. Zhang, and L. Yu, "Robust predictive tracking control for mobile robots with intermittent measurement and quantization," *IEEE Trans. Ind. Electron.*, vol. 68, no. 1, pp. 509–518, Jan. 2021.

[23] A. Liu, W.-A. Zhang, L. Yu, H. Yan, and R. Zhang, "Formation control of multiple mobile robots incorporating an extended state observer and distributed model predictive approach," *IEEE Trans. Syst., Man, Cybern., Syst.*, vol. 50, no. 11, pp. 4587–4597, Nov. 2020.

[24] L. Dai, Y. Xia, Y. Gao, and M. Cannon, "Distributed stochastic MPC of linear systems with additive uncertainty and coupled probabilistic constraints," *IEEE Trans. Autom. Control*, vol. 62, no. 7, pp. 3474–3481, Jul. 2017.

[25] A. Nikou, C. Verginis, S. Heshmati-Alamdari, and D. V. Dimarogonas, "A nonlinear model predictive control scheme for cooperative manipulation with singularity and collision avoidance," in *Proc. 25th Mediterr. Conf. Control Autom. (MED)*, 2017, pp. 707–712, doi: 10.1109/MED.2017.7984201.

[26] S. Heshmati-Alamdari, G. C. Karras, and K. J. Kyriakopoulos, "A distributed predictive control approach for cooperative manipulation of multiple underwater vehicle manipulator systems," in *Proc. Int. Conf. Robot. Autom. (ICRA)*, 2019, pp. 4626–4632.

[27] D. Qin, A. Liu, D. Zhang, and H. Ni, "Formation control of mobile robot systems incorporating primal-dual neural network and distributed predictive approach," *J. Franklin Inst.*, vol. 357, no. 17, pp. 12454–12472, Nov. 2020.

[28] Y. Zhang, W. Ma, X.-D. Li, H.-Z. Tan, and K. Chen, "MATLAB simulink modeling and simulation of LVI-based primal–dual neural network for solving linear and quadratic programs," *Neurocomputing*, vol. 72, nos. 7–9, pp. 1679–1687, Mar. 2009.

[29] Y. Xia and J. Wang, "A general projection neural network for solving optimization and related problems," in *Proc. Int. Joint Conf. Neural Netw.*, vol. 3, Jul. 2003, pp. 2334–2339.

[30] X. Hu, "Applications of the general projection neural network in solving extended linear-quadratic programming problems with linear constraints," *Neurocomputing*, vol. 72, nos. 4–6, pp. 1131–1137, Jan. 2009.

[31] H. Xiao and C. L. P. Chen, "Incremental updating multirobot formation using nonlinear model predictive control method with general projection neural network," *IEEE Trans. Ind. Electron.*, vol. 66, no. 6, pp. 4502–4512, Jun. 2019.

[32] X. Hu and J. Wang, "Solving generally constrained generalized linear variational inequalities using the general projection neural networks," *IEEE Trans. Neural Netw.*, vol. 18, no. 6, pp. 1697–1708, Nov. 2007.

[33] G. D. White, R. M. Bhatt, C. P. Tang, and V. N. Krovi, "Experimental evaluation of dynamic redundancy resolution in a nonholonomic wheeled mobile manipulator," *IEEE/ASME Trans. Mechatronics*, vol. 14, no. 3, pp. 349–357, Jun. 2009.

[34] D. Williams and O. Khatib, "The virtual linkage: A model for internal forces in multi-grasp manipulation," in *Proc. IEEE Int. Conf. Robot. Autom.*, vol. 1, 1993, pp. 1025–1030, doi: 10.1109/ROBOT.1993.292110.

[35] J.-W. Lee, W.-H. Kwon, and J. Choi, "On stability of constrained receding horizon control with finite terminal weighting matrix," *Automatica*, vol. 34, no. 12, pp. 1607–1612, Jun. 1998.

[36] H. Chen and F. Allgöwer, "A quasi-infinite horizon nonlinear model predictive control scheme with guaranteed stability," *Automatica*, vol. 34, no. 10, pp. 1205–1217, Oct. 1998.

Authorized licensed use limited to: b-on: Universidade de Lisboa Reitoria. Downloaded on October 20,2024 at 11:23:04 UTC from IEEE Xplore. Restrictions apply.

Dongdong Qin received the B.Eng. degree from the Department of Automation, Huangshan University, Huangshan, China, in 2018. He is currently pursuing the Ph.D. degree with the College of Automation Science and Engineering, Zhejiang University of Technology, Hangzhou, China.

His research interests include distributed model predictive control, cooperation control, and networked multirobot system.

Jinhui Wu received the B.Eng. degree in electrical engineering and automation from Zhejiang University of Science and Technology, Hangzhou, China, in 2017, where he is currently pursuing the Ph.D. with the College of Automation Science and Engineering.

His research interests include distributed model predictive control, cooperation control, and networked multirobot system.

Andong Liu received the B.Eng. degree in automation from Guangxi University, Nanning, China, in 2007, and the Ph.D. degree in control theory and control engineering from Zhejiang University of Technology, Hangzhou, China, in 2014.

He is currently an Associate Professor with the Department of Automation, College of Information Engineering, Zhejiang University of Technology. He was a Postdoctoral Research Fellow with the Department of Electronic Engineering, City University of Hong Kong, Hong Kong, from 2016 to 2018. His research interests include model predictive control, networked control systems, and mobile robots.

Wen-An Zhang (Member, IEEE) received the B.Eng. degree in automation and the Ph.D. degree in control theory and control engineering from Zhejiang University of Technology, Hangzhou, China, in 2004 and 2010, respectively.

He has been with Zhejiang University of Technology since 2010 where he is currently a Professor with the Department of Automation. He was a Senior Research Associate with the Department of Manufacturing Engineering and Engineering Management, City University of Hong Kong, Hong Kong, from 2010 to 2011. He was awarded an Alexander von Humboldt Fellowship in 2011–2012. His research interests include networked control systems, multisensor information fusion estimation, and robotics.

Prof. Zhang has been serving as a Subject Editor for *Optimal Control Applications and Methods* from September 2016.

Li Yu (Member, IEEE) received the B.S. degree in control theory from Nankai University, Tianjin, China, in 1982, and the M.S. and Ph.D. degrees from Zhejiang University, Hangzhou, China, in 1988 and 1999, respectively.

He is currently a Professor with the College of Information Engineering, Zhejiang University of Technology, Hangzhou. He has authored or coauthored three books and over 200 journal or conference papers. His research interests include wireless sensor networks, networked control systems, and motion control.

Authorized licensed use limited to: b-on: Universidade de Lisboa Reitoria. Downloaded on October 20,2024 at 11:23:04 UTC from IEEE Xplore. Restrictions apply.